R. & M. No. 3171
20,301
A.R.C. Technical Report

MINISTRY OF AVIATION

AERONAUTICAL RESEARCH COUNCIL
REPORTS AND MEMORANDA

Aerodynamic Derivative Measurements on a Rectangular Wing of Aspect Ratio 3·3

By P. R. GUYETT, B.Sc. and J. K. CURRAN

LONDON: HER MAJESTY'S STATIONERY OFFICE
1961
PRICE 9*s.* 6*d.* NET

Aerodynamic Derivative Measurements on a Rectangular Wing of Aspect Ratio 3·3

By P. R. GUYETT, B.Sc. and J. K. CURRAN

COMMUNICATED BY THE DEPUTY CONTROLLER AIRCRAFT (RESEARCH AND DEVELOPMENT)
MINISTRY OF AVIATION

*Reports and Memoranda No. 3171**
March, 1958

Summary. A complete set of oscillatory aerodynamic stiffness and damping derivatives has been determined for a rectangular wing for rigid-wing modes of normal translation, pitch, and roll, in the range of frequency parameter 0·4 to 1·3, at low subsonic wind speeds. Each available comparison shows that the results are in satisfactory agreement with theoretical derivatives calculated by W. P. Jones and by Lawrence and Gerber.

1. *Introduction.* Increasing attention is now being given to the problem of determining the aerodynamic derivatives to be used in flutter calculations. Both the theoretical and the experimental approaches are difficult, and in theoretical calculations important simplifying assumptions are usually made. At present, there is more theoretical than experimental information available. As a consequence, more experimental work is needed to assess the accuracy of the existing theoretical results, as well as to provide data for direct use in flutter calculations.

This report describes wind-tunnel measurements of derivatives for a rectangular wing of aspect ratio 3·3 at low subsonic wind speeds. Derivatives were found for rigid-wing modes of normal translation, pitch, and roll, in the range of frequency parameter 0·4 to 1·3. The Reynolds number varied between $0{\cdot}4 \times 10^6$ at frequency parameter 1·3, and $1{\cdot}5 \times 10^6$ at frequency parameter 0·4. Theoretical results for certain of these modes have been calculated by W. P. Jones[1] and by Lawrence and Gerber[2], and comparison shows that there is fairly good agreement between the theoretical and experimental results.

2. *Method.* The position of a rigid wing may be conveniently specified in terms of its displacement in normal translation, angle of pitch, and angle of roll. The aerodynamic derivatives appropriate to each of these forms of motion can be found from a series of tests in which the wing is oscillated with these motions either separately or in combination. In the present tests the chosen modes of oscillation were pitch about the wing leading edge, pitch about the trailing edge, and roll about a chordwise axis near the root.

In each of these modes the lift force, pitching moment, and rolling moment were measured over a range of frequency parameter during sustained oscillations. The required forces and moments were found from the outputs of force transducers mounted on the axis of oscillation and from the output of a single force transducer mounted in a link providing the excitation about the axis. The reactions of the wing inertia forces at the force measuring points were reduced by mounting the

* R.A.E. Report Structures 235, received 10th July, 1958.

wing on a system of springs. The springs were arranged to give the required balance of forces at a chosen frequency of oscillation and this frequency was maintained throughout the tests. Variation of frequency parameter was obtained by altering the wind speed.

Details of the use of springs to reduce inertia force reactions have been given in an earlier report[3]. There the method was used to obtain a balance of pitching moments only; in the present work the method was extended to provide a balance of total force, pitching moment and rolling moment. The required spring stiffnesses and positions may be found as follows:

Consider the wing shown in Fig. 1. Three equations of motion for rigid body pitch about the axis are obtained:

Applied external normal force

$$= M\bar{x}\ddot{\theta} + K_1x_1\theta + K_2x_2\theta + \ldots. + D_1\dot{\theta}.$$

Applied external pitching moment

$$= I_y\ddot{\theta} + K_1x_1^2\theta + K_2x_2^2\theta + \ldots. + D_2\dot{\theta}\,.$$

Applied external rolling moment

$$= I_{xy}\ddot{\theta} + K_1x_1y_1\theta + K_2x_2y_2\theta + \ldots. + D_3\dot{\theta}\,.$$

If the wing performs simple harmonic motion at circular frequency ω, then $\theta = \bar{\theta}\,e^{i\omega t}$ and $\ddot{\theta} = -\omega^2\theta$.

Hence the equations become:

Applied external normal force

$$= (-\omega^2M\bar{x} + K_1x_1 + K_2x_2 + \ldots.)\,\theta + i\omega D_1\theta\,.$$

Applied external pitching moment

$$= (-\omega^2I_y + K_1x_1^2 + K_2x_2^2 + \ldots.)\,\theta + i\omega D_2\theta\,.$$

Applied external rolling moment

$$= (-\omega^2I_{xy} + K_1x_1y_1 + K_2x_2y_2 + \ldots.)\,\theta + i\omega D_3\theta\,.$$

Now the spring positions and stiffnesses may be chosen to make

$$(-\omega^2M\bar{x} + K_1x_1 + K_2x_2 + \ldots.) = 0\,,$$

$$(-\omega^2I_y + K_1x_1^2 + K_2x_2^2 + \ldots.) = 0\,,$$

$$(-\omega^2I_{xy} + K_1x_1y_1 + K_2x_2y_2 + \ldots.) = 0\,.$$

External forces are thus required solely to overcome the still air damping of the system. If the wing is then oscillated in a wind stream at the same frequency ω, the additional forces required (which will in general be large compared with the still air forces) give directly the additional aerodynamic forces acting on the wing.

3. *Apparatus.* 3.1. *Wind Tunnel.* The tests were made in the Royal Aircraft Establishment 5 ft Diameter Low Speed Wind Tunnel. The open working-section of the tunnel was closed for this experiment by fitting a circular-section tube between the entry nozzle and the safety screen. A fairing was built into the bottom of the tube to give a horizontal flat surface at the model position. Fig. 2 shows the arrangement.

3.2. *Wing Model and Support.* The wing projected vertically into the wind stream through a slot in the fairing at the bottom of the working-section and for each test was set at a mean incidence of 0 deg. The wing was of rectangular plan-form with a chord of 20 in. and had a wind swept length of 33·5 in. giving a full-span aspect ratio of 3·35. The wing section was symmetrical, to RAE 101 profile, with a 0·10 thickness/chord ratio. A built-up construction was used, with two spars of spruce and plywood, plywood ribs, spruce leading-edge and trailing-edge members, and a plywood skin stiffened with balsa. The spars were extended to form a rectangular-section root block.

The root block was bolted into a frame of Duralumin angle which was supported by two cross-spring bearings (Fig. 2). The bearings were attached to a heavy frame beneath the wind tunnel and could be positioned to allow the wing to pitch about either its leading edge or trailing edge or roll about an axis below the wing root. In the two pitching modes a further bearing was fixed at the wing tip on the axis of oscillation to increase the wing bending stiffness.

To reduce the airflow through the slot at the wing root during the pitching oscillations, a horizontal metal plate overlapping the slot was attached to the wing and oscillated with it. In the rolling oscillation the motion of the wing at the wall surface was small and the airflow was limited by a metal cover plate, fixed to the fairing, which had a cut-out shaped closely to the wing contour. A second plate, shaped so that its surface formed a radius about the roll axis, was fixed to the wing below the tunnel wall, and increased the length of the leakage path.

3.3. *Excitation System.* In each mode the oscillation was maintained by forcing the wing from a swash-plate exciter (Fig. 3). The angle of tilt of the swash plate could be varied smoothly to alter the amplitude of oscillation of a plunger rod projecting from the exciter body. Sinusoidal forcing from the plunger was transmitted through a spring and parallel linkage support to a rod coupled to the mid-chord point of the wing approximately two thirds of the span from the root.

3.4. *Frequency Measurement.* From Section 2 it may be seen that the balance between the wing inertia loads and the spring reactions occurs at one frequency only for a given arrangement of springs. For correct measurement of the superimposed forces this chosen frequency must therefore be accurately maintained. To ensure this, the frequency was recorded at approximately 10 sec intervals throughout the test by means of an electronic counter, and when necessary, corrected by manually adjusting the speed of the exciter motor.

The electronic counter[4] measured the frequency to an accuracy of about $\pm$ 0·05 per cent and generally the frequency was maintained to within $\pm$ 0·1 per cent of the chosen value.

3.5. *Force Measurement and Recording.* Applied forces normal to the mean plane of the wing were measured by force transducers mounted at each hinge point on the wing axis of oscillation and in the linkage system from the exciter. Fig. 3 shows their position for a pitching mode.

Details of a typical force transducer are given in Fig. 4. The two beryllium copper strips were pretensioned by tightening the bolts in the centre connector and under axial load the tension in one strip increased and the tension in the other decreased. Wire-resistance strain-gauges cemented to the strips formed a Wheatstone bridge sensitive to loading in the axial direction.

Output from the galvanometer arm of the Wheatstone bridge was supplied to one of two pairs of brushes bearing at 180 deg on a two segment commutator mounted on the shaft of the exciter and rotating at the wing oscillation frequency. Each of the two commutator segments had an outer

slip ring which was connected to the galvanometer. Fig. 5 shows the arrangement. The transducer output was thus reversed in direction at half cycle intervals to produce a signal having a mean D.C. level which was measured by the galvanometer. The transducer output could also be switched to the second pair of brushes, at 90 deg to the first pair. The forms of the resulting signals are indicated in Fig. 6. It may be shown that the galvanometer response to a sinusoidal signal is as follows:

From 1st pair of brushes:

$$\text{Reading} = -\frac{2}{\pi} S_0 \cos \psi .$$

From 2nd pair of brushes:

$$\text{Reading} = \frac{2}{\pi} S_0 \sin \psi .$$

The two readings thus enabled the amplitude of the transducer output and its phase relationship to the commutator to be found. Due, however, to the filtering spring in the exciter linkage the commutator rotation was not at a fixed phase angle with the wing. A strain-gauged cantilever strip was therefore connected to the wing and its gauge output was also supplied to the commutator and measured at the galvanometer. The cantilever produced a signal in phase with the wing displacement and from the two sets of measurements the components of the transducer output in phase and in quadrature with the wing motion were found.

4. *Test Procedure.* In each mode the reactions of the wing inertia forces at the force transducer points were reduced by forcing the wing to oscillate against springs, as described in Section 2. The frequency of oscillation chosen was 4·98 c.p.s. A precise balance of force at this frequency was not attempted, since the process of making small changes in spring stiffness and position was laborious, but instead the inertia reactions were brought well below the level of the aerodynamic forces. These residual forces, in phase with the motion, and the accompanying quadrature forces required to overcome the structural and aerodynamic damping were then measured in still air at the chosen frequency and amplitude of oscillation. Measurements were then made at the same frequency and amplitude at wind speeds of 40, 60, 80, 100, 120, 140 ft/sec. Following the wind-on tests a further set of measurements was made in still air. The aerodynamic forces due to the wind stream at each speed were taken to be the difference between the wind-on and still-air force measurements.

The in-phase forces found in this way correspond to the aerodynamic forces due to displacement alone, since the virtual inertia forces, which are present both with the wind on and in still air, are excluded by the subtraction. Similarly the derived forces in quadrature with the wing motion do not include the still-air aerodynamic damping.

Two sets of measurements were made in each mode of oscillation, under nominally identical conditions, to indicate how consistent were the experimental results.

The force transducers were calibrated dynamically whenever possible by attaching masses to the wing and measuring the additional outputs in an oscillation at the test frequency and amplitude. In the rolling mode the forces arising at the two transducer points on the axis of oscillation and at the transducer in the exciter linkage were uniquely determined by the magnitude and position of the attached mass. In the pitching modes a similar direct calibration was made of the transducer in the exciter linkage but the three transducers on the axis of oscillation created a redundant support

and prevented complete direct calibration. Those at the hinge points were therefore mounted in turn on a rigid structure in line with the exciter linkage and force applied by the exciter through the filtering spring to the linkage and the hinge-point transducers. Both outputs were then measured and the ratio of their sensitivities found. The required absolute calibrations were subsequently determined from the known calibration of the linkage transducer.

5. *Presentation of Results.* The measured forces and moments have been expressed in terms of equivalent constant strip derivatives. These are defined as derivatives which are chosen to be independent of spanwise position but which when integrated over the wing in the appropriate mode give the correct generalised forces.

The derivatives are evaluated for reference axes at the wing leading edge and wing root.

The damping derivatives given do not include the effect of the still-air aerodynamic damping (*see* Section 4). It has been shown[3] that the still-air damping coefficient, in general, depends upon the frequency and amplitude of the motion, and represents only a very small addition to the measured values.

5.1. *Pitch about the Leading Edge.* For the chosen reference axes this mode involved pitching displacement only.

$$\text{Lift} = \int_0^s \rho V^2 c\, dy\, (l_\alpha + ivl_{\dot\alpha})\alpha = \rho V^2 S\alpha(l_\alpha + ivl_{\dot\alpha}) .$$

$$\text{Pitching moment about leading edge} = \int_0^s \rho V^2 c^2\, dy\, (m_\alpha + ivm_{\dot\alpha})\alpha = \rho V^2 Sc\alpha(m_\alpha + ivm_{\dot\alpha}) .$$

$$\text{Rolling moment} = \int_0^s \rho V^2 c\, dy\, y(n_\alpha + ivn_{\dot\alpha})\alpha = \tfrac{1}{2}\rho V^2 Ss\alpha(n_\alpha + ivn_{\dot\alpha}) .$$

The above derivatives, l_α, $l_{\dot\alpha}$, m_α, $m_{\dot\alpha}$, n_α, $n_{\dot\alpha}$, are given in Table 1 and are plotted against frequency parameter in Figs. 8 to 10.

5.2. *Pitch about the Trailing Edge.* In this mode, displacements in pitch and normal translation occurred simultaneously, with $z/c = -\alpha$.

$$\begin{aligned}\text{Lift} &= \int_0^s \rho V^2 c\, dy\, \{(l_\alpha + ivl_{\dot\alpha}) - (l_z + ivl_{\dot z})\}\,\alpha \\ &= \rho V^2 S\alpha\, \{(l_\alpha + ivl_{\dot\alpha}) - (l_z + ivl_{\dot z})\} .\end{aligned}$$

$$\begin{aligned}\text{Pitching moment about leading edge} &= \int_0^s \rho V^2 c^2\, dy\, \{(m_\alpha + ivm_{\dot\alpha}) - (m_z + ivm_{\dot z})\}\,\alpha \\ &= \rho V^2 Sc\alpha\, \{(m_\alpha + ivm_{\dot\alpha}) - (m_z + ivm_{\dot z})\} .\end{aligned}$$

$$\begin{aligned}\text{Rolling moment} &= \int_0^s \rho V^2 c\, dy\, y\, \{(n_\alpha + ivn_{\dot\alpha}) - (n_z + ivn_{\dot z})\}\,\alpha \\ &= \tfrac{1}{2}\rho V^2 Ss\alpha\, \{(n_\alpha + ivn_{\dot\alpha}) - (n_z + ivn_{\dot z})\} .\end{aligned}$$

The above combinations of derivatives $(l_\alpha - l_z)$, $(l_{\dot\alpha} - l_{\dot z})$ . . . are given in Table 2, and are plotted against frequency parameter in Figs. 11 to 13.

From the mean curves in Figs. 8 to 13 the derivatives for displacement alone, l_z, $l_{\dot z}$, . . . were found and are plotted in Figs. 14 to 16.

5.3. *Roll about an Axis Inboard of the Wing Root.* The test rolling mode contained the reference modes of roll about the root and normal translation. The displacement in normal translation, equalled the displacement at the wing root, *i.e.*,

$$z' = r\phi ,$$

where r = distance of the test roll axis below the wing root (4·40 in.).

$$\text{Lift} = \int_0^s \rho V^2 c\, dy\, (l_\phi + ivl_{\dot\phi}) \frac{y\phi}{c} + \int_0^s \rho V^2 c\, dy\, (l_z + ivl_{\dot z}) \frac{z'}{c}$$

$$= \tfrac{1}{2}\rho V^2 s^2 \phi (l_\phi + ivl_{\dot\phi}) + \rho V^2 sc \frac{z'}{c}(l_z + ivl_{\dot z})$$

$$= \tfrac{1}{2}\rho V^2 s^2 \phi \left\{ (l_\phi + ivl_{\dot\phi}) + 2\frac{r}{s}(l_z + ivl_{\dot z}) \right\} .$$

Pitching moment about the leading edge

$$= \int_0^s \rho V^2 c^2\, dy\, (m_\phi + ivm_{\dot\phi}) \frac{y\phi}{c} + \int_0^s \rho V^2 c^2\, dy\, (m_z + ivm_{\dot z}) \frac{z'}{c}$$

$$= \tfrac{1}{2}\rho V^2 s^2 c\phi (m_\phi + ivm_{\dot\phi}) + \rho V^2 sc^2 \frac{z'}{c}(m_z + ivm_{\dot z})$$

$$= \tfrac{1}{2}\rho V^2 s^2 c\phi \left\{ (m_\phi + ivm_{\dot\phi}) + 2\frac{r}{s}(m_z + ivm_{\dot z}) \right\} .$$

$$\text{Rolling moment} = \int_0^s \rho V^2 c\, dy\, y(n_\phi + ivn_{\dot\phi}) \frac{y\phi}{c} + \int_0^s \rho V^2 c\, dy\, y(n_z - ivn_{\dot z}) \frac{z'}{c}$$

$$= \tfrac{1}{3}\rho V^2 s^3 \phi (n_\phi + ivn_{\dot\phi}) + \tfrac{1}{2}\rho V^2 s^2 c \frac{z'}{c}(n_z + ivn_{\dot z})$$

$$= \tfrac{1}{3}\rho V^2 s^3 \phi \left\{ (n_\phi + ivn_{\dot\phi}) + \frac{3}{2}\frac{r}{s}(n_z + ivn_{\dot z}) \right\} .$$

The above combinations of derivatives, $l_\phi + 2(r/s)l_z$, . . . are given in Table 3 and are plotted against frequency parameter in Figs. 17 to 19.

From these results and the displacement derivatives given in Figs. 14 to 16, values for the roll derivatives l_ϕ, $l_{\dot\phi}$, . . . were found and are plotted in Figs. 20 to 22.

6. *Discussion of Results and Comparison with Theory.* The measured derivatives are shown plotted against frequency parameter in Figs. 8 to 22. Wherever possible the graphs include corresponding theoretical values. These theoretical derivatives have been extrapolated from the calculated values at aspect ratios 4 and 6 given by W. P. Jones[1], or interpolated from values obtained by Minhinnick (R.A.E.) from the work of Lawrence and Gerber[2]. The theoretical derivatives for roll, in Fig. 22, were obtained from results for a symmetric mode of oscillation, since the tunnel wall was considered to act as a reflector plate and produce a plane of symmetry at the wing root.

6.1. *Pitch about the Leading Edge* (*Figs.* 8 *to* 10). All the measured stiffness and damping derivatives show only small variation over the test range of frequency parameter. A measured value for the static pitching-moment derivative (m_α at $\nu = 0$) is in close agreement with the oscillatory values and suggests that the stiffness derivatives are practically independent of frequency parameter

over the whole range $\nu = 0$ to $1{\cdot}4$. The theoretical derivatives also show comparatively small variation with frequency parameter. The stiffness derivatives, however, tend to maximum values at zero frequency parameter, although this is less marked with the Lawrence and Gerber derivatives. Comparison shows that the values of the measured stiffness derivatives are higher than the corresponding theoretical derivatives. A part at least of this discrepancy probably arises from the constraint imposed upon the wind stream by the wind-tunnel walls. Theoretical wind-tunnel wall corrections are available for certain configurations, but not, so far as the writers know, for the particular boundaries of the present tests. A simplified calculation was therefore made (*see* Appendix) to obtain an approximation to the static corrections applying under the test conditions, since these should give a good indication of the correction that should be made to the stiffness derivatives. The calculation shows that the measured static values would be higher than the free-stream values by 7 per cent. With this correction applied, the measured l_α derivatives agree closely with the corresponding theoretical derivatives for frequency parameters greater than $0{\cdot}4$,and the measured m_α derivatives have slightly higher values than the corresponding theoretical derivatives. A wind-tunnel correction should also be applied to the measured damping derivatives. W. P. Jones[5] has calculated these corrections for a rectangular wing in a closed rectangular working-section tunnel, and shows that the derivatives $l_{\dot\alpha}$ and $m_{\dot\alpha}$ in the presence of the walls are slightly smaller than the free-stream values. Acum and Garner[6] have also shown that the corrections to the damping derivatives for a swept wing in a circular tunnel are negligible. Neither of these calculations apply to the test conditions but suggest that the corrections are small. The experimental and theoretical derivatives may therefore be considered in good agreement.

6.2. *Pitch about the Trailing Edge* (*Figs.* 11 *to* 13). The lift forces, pitching moments, and rolling moments acting in the oscillation about the trailing edge were obtained from what were generally small differences of large forces measured at the four transducer positions. The experimental accuracy was consequently less than in the condition for oscillation about the leading edge, where the transducer positions were more favourable, and gave rise to some experimental scatter. Nevertheless, the measured derivatives are in substantial agreement with theory, especially in view of the wind-tunnel wall-constraint corrections which probably reduce the magnitude of the measured stiffness derivatives.

6.3. *Normal Translation* (*Figs.* 14 *to* 16). The derivatives for normal translation were obtained by subtracting the results for pitch about the trailing edge from the results for pitch about the leading edge (*see* Section 5).

This method gives rise to a fairly low accuracy in the values determined for the stiffness derivatives l_z, m_z and n_z since these are small by comparison with the pitching stiffness derivatives. In particular, physical considerations suggest that the variation of the derivatives with frequency parameter is more linear than the results indicate. There is, however, fairly good general agreement with theory in view of the probable experimental errors, and in any case these derivatives are not very important in flutter calculations.

The corresponding damping derivatives are in satisfactory agreement with theory. The derivative $l_{\dot z}$ has also been measured by Buchan, Harris and Somervail[7] for rectangular wings of aspect ratios 3, 4 and 5. Their results were approximately 10 per cent lower than the theoretical values of W. P. Jones and this was ascribed to the effect of the 22 deg trailing-edge angle of their aerofoil.

The trailing-edge angle of the R.A.E. test wing, 10 deg was a closer approximation to the theoretical, flat-plate condition and the present results are in closer agreement with theory.

6.4. *Roll* (*Figs.* 17 *to* 22). The measured derivatives for the rolling oscillation about an axis below the wing root are given in Figs. 17 to 19, and the derivatives for roll about the root, which were obtained from these derivatives and the normal translation derivatives, are given in Figs. 20 to 22.

The stiffness forces present in the rolling mode were small by comparison with the damping forces and it was consequently difficult to resolve the stiffness forces accurately. The resulting derivatives, l_ϕ, m_ϕ, n_ϕ, however, are generally unimportant in flutter calculations, in the same way as the stiffness derivatives in normal translation are considered generally unimportant.

The direct damping in roll derivative, $n_{\dot{\phi}}$, is in satisfactory agreement with theory although at low-frequency parameters the measured derivative is slightly greater in magnitude than the corresponding theoretical values. Bratt and Wight[8] have measured this derivative on a rectangular wing of aspect ratio 6 and their results are also slightly higher than the theoretical derivatives of W. P. Jones, and are thus consistent with the present results.

7. *Conclusions.* Oscillatory aerodynamic stiffness and damping derivatives have been measured on a rectangular wing of aspect ratio 3·3 for rigid modes of normal translation, pitch and roll. The results cover the range of frequency parameter 0·4 to 1·3 at low subsonic wind speeds. Within this range the derivatives most significant in flutter calculations show only small variations with frequency parameter. Comparison with theoretical results calculated by W. P. Jones and by Lawrence and Gerber show that small differences exist between the two sets of theoretical results but there is satisfactory general agreement with the experimental results. The constraint imposed upon the wind stream by the walls of the wind tunnel leads to uncertainties in the experimental results; and a precise evaluation of the relative accuracy of the two sets of theoretical results on the basis of the experiments cannot be made.

Acknowledgement. The authors wish to acknowledge the assistance given by D. E. G. Poulter, R.A.E., in the preparation of the equipment for these tests.

NOTATION

M	Mass of the wing
$\bar{x}$	Distance of wing c.g. from axis of oscillation
θ	Angle of pitch
$\bar{\theta}$	Amplitude in pitch
I_y	Inertia of wing about axis of pitch
I_{xy}	Product of inertia of wing about reference axes
K	Spring stiffness
D_1	Dimensional coefficient of normal force due to structural and still-air aerodynamic damping
D_2	Dimensional coefficient of pitching moment due to structural and still-air aerodynamic damping
D_3	Dimensional coefficient of rolling moment due to structural and still-air aerodynamic damping
ω	Circular frequency of oscillation
S_0	Amplitude of transducer output
ψ	Phase angle between commutator rotation and transducer output
ρ	Air density
V	Wind speed
c	Wing chord
s	Wing length from root to tip
S	Wing area ($S = sc$)
y	Distance of typical chordwise strip from wing root
ν	Frequency parameter ($\nu = \omega c/V$)
z	Displacement in normal translation. Positive downwards
α	Angle of pitch about leading edge. Positive angle nose up
ϕ	Angle of roll about root. Positive tip downwards
l_z, l_α, l_ϕ	Non-dimensional lift stiffness derivatives for motion in normal translation, pitch, roll respectively
$l_{\dot{z}}$, $l_{\dot{\alpha}}$, $l_{\dot{\phi}}$	Non-dimensional lift damping derivatives for motion in normal translation, pitch, roll respectively. Lift direction positive upwards
m_z, m_α, m_ϕ	Non-dimensional pitching-moment stiffness derivatives for motion in normal translation, pitch, roll respectively
$m_{\dot{z}}$, $m_{\dot{\alpha}}$, $m_{\dot{\phi}}$	Non-dimensional pitching-moment damping derivatives for motion in normal translation, pitch, roll respectively. Pitching moment measured about leading edge, positive nose up
n_z, n_α, n_ϕ	Non-dimensional rolling-moment stiffness derivatives for motion in normal translation, pitch, roll respectively
$n_{\dot{z}}$, $n_{\dot{\alpha}}$, $n_{\dot{\phi}}$	Non-dimensional rolling-moment damping derivatives for motion in normal translation, pitch, roll respectively. Rolling moment measured about wing root, positive tip downwards

REFERENCES

No.	*Author*	*Title, etc.*
1	W. P. Jones	Theoretical airload and derivative coefficients for rectangular wings. R. & M. 2142. February, 1943.
2	H. R. Lawrence and E. H. Gerber	The aerodynamic forces on low-aspect-ratio wings oscillating in an incompressible flow. *J. Ae. Sci.* Vol. 19. No. 11. November, 1952.
3	P. R. Guyett and D. E. G. Poulter	Measurements of pitching-moment derivatives for a series of rectangular wings at low wind speeds. C. P. 249. June, 1955.
4	W. D. T. Hicks	An electronic instrument for the accurate measurement of the frequency of structural oscillations. A.R.C. 17,920. January, 1955.
5	W. P. Jones	Wind-tunnel interference effect on the values of experimentally determined derivative coefficients for oscillating aerofoils. R. & M. 1912. August, 1943.
6	W. E. Acum and H. C. Garner ..	Approximate wall corrections for an oscillating swept wing in a wind tunnel of closed circular section. C. P. 184. January, 1954.
7	A. L. Buchan, K. D. Harris and P. M. Somervail	Measurement of the derivative z_{ω} for an oscillating aerofoil. The College of Aeronautics, Cranfield, Report 40 A.R.C. 13,548. June, 1950.
8	J. B. Bratt and K. C. Wight ..	The effect of sweepback on the fundamental derivative coefficient for flexural motion. R. & M. 2774. October, 1950.
9	H. Glauert	*The Elements of Aerofoil and Airscrew Theory*. Ch. XIV. 2nd Edition. Cambridge University Press. 1948.

APPENDIX

Approximate Steady-State Correction for the Effect of the Tunnel Walls

Following the method given by Glauert[9] let the wing be represented by a line vortex, of strength K, with trailing vortices at the wing tips. Fig. 7 shows the system in section. It is required to find the downwash velocity at the centre of the wing when the tunnel wall is a streamline.

By transforming the region within the boundary into a half plane the problem is simplified, and the following solution is obtained:

Total downwash at the centre of the wing

$$= \frac{K}{2b\gamma} \cot \left\{ \left(\frac{\pi}{2} + \beta \right) \frac{\pi}{2\gamma} \right\},$$

where

$$\tan \beta = \frac{s^2 - b^2}{2bs},$$

$$\tan \gamma = - \frac{2ab}{a^2 - b^2},$$

and a, b and s are wind-tunnel and wing dimensions given in Fig. 7.

Now, the downwash at the centre of the wing in a free stream due to the two semi-infinite tip vortices $= K/(2\pi s)$.

Hence the upwash velocity due to the walls,

$$w = \frac{K}{2\pi s} - \frac{K}{2b\gamma} \cot \left\{ \left(\frac{\pi}{2} + \beta \right) \frac{\pi}{2\gamma} \right\} = \sigma K,$$

where

$$\sigma = \frac{1}{2\pi s} - \frac{1}{2b\gamma} \cot \left\{ \left(\frac{\pi}{2} + \beta \right) \frac{\pi}{2\gamma} \right\}.$$

Now wing lift

$$= 2s\rho KV = \rho V^2 A \, l_\alpha \, \alpha,$$

where A is the total wing area $= 2sc$.

Hence

$$K = V c \, l_\alpha \, \alpha.$$

The upward inclination of the stream due to the walls,

$$\epsilon = \frac{w}{V} = \frac{\sigma K}{V} = \sigma c \, l_\alpha \, \alpha.$$

Thus the true wing incidence

$$= \epsilon + \alpha.$$

In the test

$$a = 4{\cdot}75 \text{ ft},$$
$$b = 1{\cdot}09 \text{ ft},$$
$$s = 2{\cdot}79 \text{ ft},$$
$$l_\alpha = 1{\cdot}75.$$

The correction to the measured derivatives then becomes

$$\frac{\alpha}{\alpha + \epsilon} = \frac{\alpha}{\alpha + \sigma c \, l_\alpha \, \alpha} = 0{\cdot}926$$

(*see* Section 6.1).

Acknowledgements. The writers wish to acknowledge the help given by D. E. Williams and Dr. D. E. Davies, R.A.E., in obtaining the above solution for the total downwash at the centre of the wing.

TABLES

All tests were made with the wing at 0 deg mean incidence.

The results given are not corrected for wing-tunnel wall interference.

The test Reynolds number varied between $0{\cdot}4 \times 10^6$ at frequency parameter $1{\cdot}3$, and $1{\cdot}5 \times 10^6$ at frequency parameter $0{\cdot}4$.

TABLE 1

Results for Pitch about the Leading Edge

Amplitude of Pitch about the Leading Edge = $0{\cdot}0362$ *radians*

ν	l_α	$l_{\dot\alpha}$	$(-m_\alpha)$	$(-m_{\dot\alpha})$	$(-n_\alpha)$	$(-n_{\dot\alpha})$
0·375	1·743 1·756	1·291 1·319	0·442 0·445	0·622 0·629	1·632 1·644	1·211 1·227
0·438	1·746 1·739	1·321 1·345	0·446 0·439	0·629 0·626	1·638 1·617	1·229 1·264
0·527	1·713 1·742	1·313 1·312	0·440 0·448	0·618 0·621	1·603 1·633	1·211 1·241
0·660	1·727 1·737	1·352 1·375	0·442 0·448	0·630 0·626	1·622 1·591	1·252 1·259
0·884	1·777 1·748	1·380 1·399	0·481 0·463	0·625 0·624	1·726 1·669	1·287 1·266
1·338	1·864 1·760	1·463 1·424	0·516 0·476	0·641 0·625	1·681 1·636	1·349 1·363

TABLE 2

Results for Pitch about the Trailing Edge

Amplitude of Pitch about the Trailing Edge = $0{\cdot}0385$ *radians*

ν	$(l_\alpha - l_z)$	$-(l_{\dot\alpha} - l_{\dot z})$	$-(m_\alpha - m_z)$	$-(m_{\dot\alpha} - m_{\dot z})$	$-(n_\alpha - n_z)$	$(n_{\dot\alpha} - n_{\dot z})$
0·375	— 1·630	— 0·204	— 0·381	— 0·377	— 1·530	— 0·423
0·438	1·617 1·620	0·211 0·377	0·405 0·396	0·350 0·264	1·520 1·536	0·312 0·320
0·527	1·640 1·642	0·258 0·193	0·416 0·410	0·288 0·318	1·553 1·518	0·389 0·298
0·660	1·604 1·605	0·165 0·128	0·411 0·415	0·313 0·324	1·477 1·551	0·278 0·273
0·884	1·545 1·603	0·037 0·067	0·399 0·436	0·311 0·319	1·458 1·475	0·101 0·188
1·338	1·383 1·491	−0·143 −0·177	0·312 0·401	0·359 0·426	1·435 1·529	−0·119 −0·021

TABLE 3

Results for Roll about an Axis Inboard of the Wing Root
Amplitude in Roll = 0·0180 radians

ν	$(l_\phi + 0{\cdot}263l_z)$	$(l_{\dot\phi} + 0{\cdot}263l_{\dot z})$	$(-m_\phi - 0{\cdot}263m_z)$	$(-m_{\dot\phi} - 0{\cdot}263m_{\dot z})$	$(-n_\phi - 0{\cdot}197n_z)$	$(-n_{\dot\phi} - 0{\cdot}197n_{\dot z})$
0·375	0·036 0·064	2·268 2·235	0·047 0·059	0·521 0·530	0·019 0·026	1·541 1·488
0·438	0·071 0·124	2·149 2·257	0·063 0·084	0·524 0·549	0·045 0·063	1·493 1·575
0·527	0·119 0·179	2·102 2·203	0·079 0·110	0·514 0·557	0·088 0·104	1·402 1·464
0·660	0·215 0·301	1·995 2·024	0·134 0·150	0·475 0·459	0·155 0·139	1·430 1·384
0·884	0·301 0·399	1·766 1·900	0·165 0·201	0·397 0·451	0·224 0·206	1·338 1·306
1·338	0·586 0·734	1·673 1·753	0·313 0·315	0·362 0·398	0·393 0·275	1·196 1·160

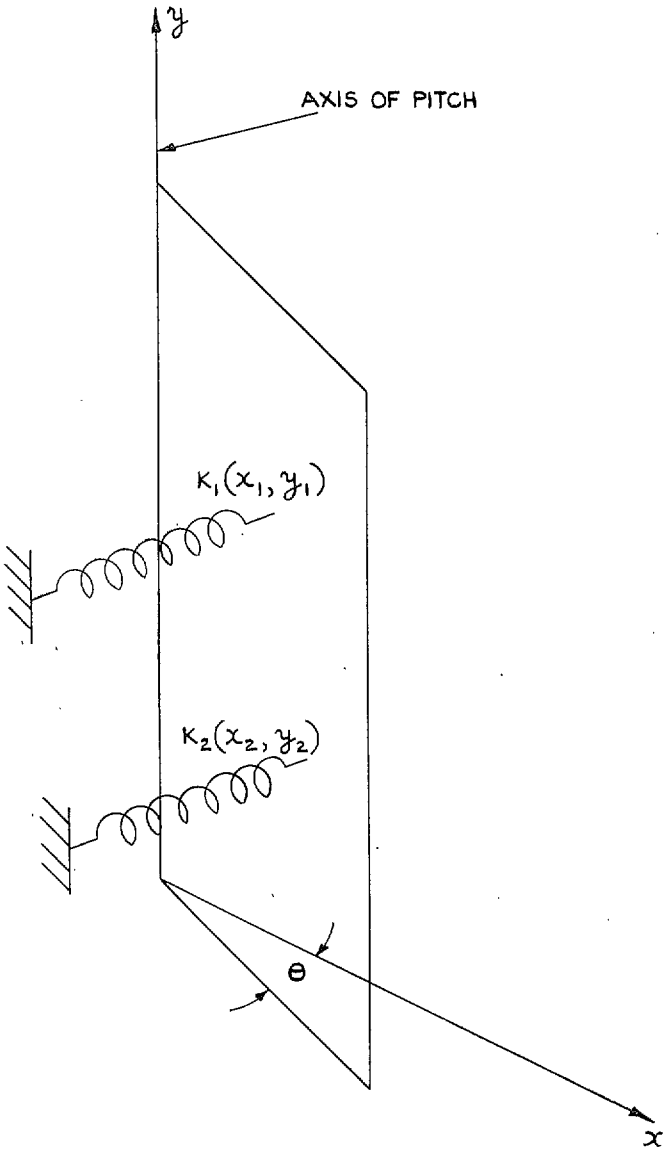

FIG. 1. Spring system for inertia balancing.

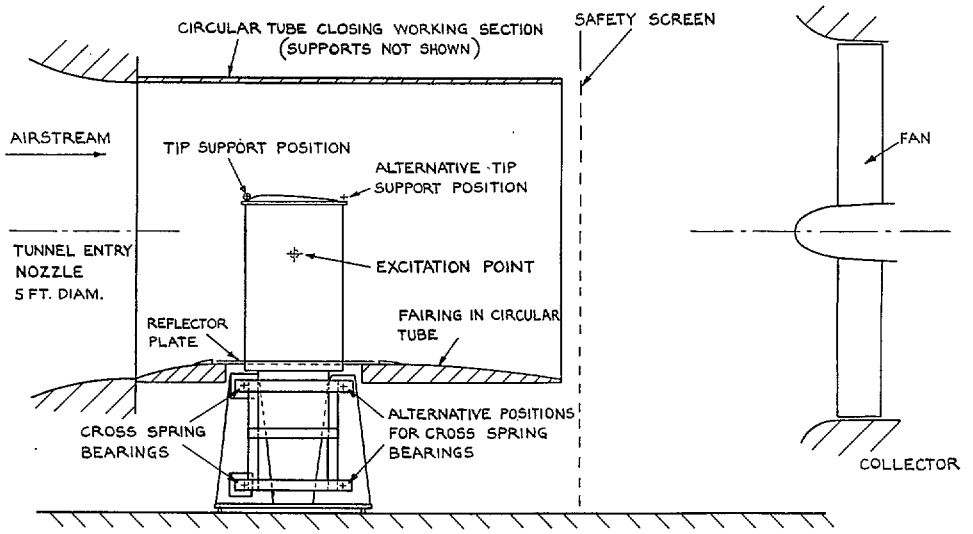

FIG. 2. Arrangement of wing in wind-tunnel working-section.

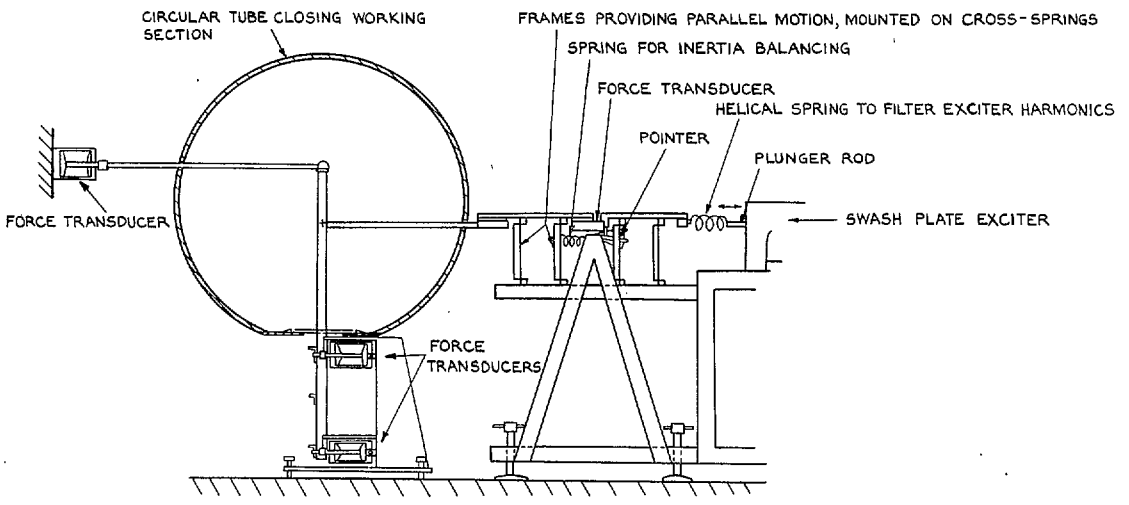

FIG. 3. Arrangement of wing and excitation equipment in wind-tunnel working-section.

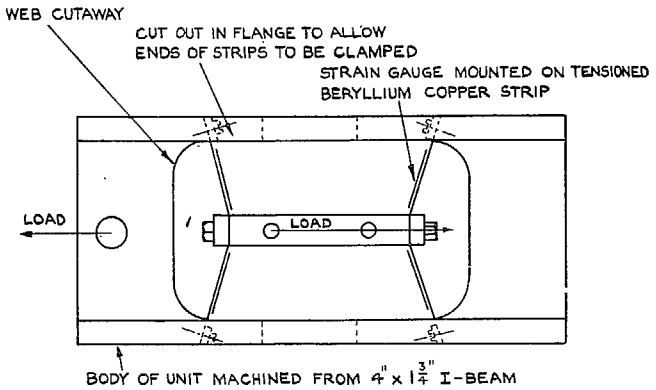

FIG. 4. Force transducer.

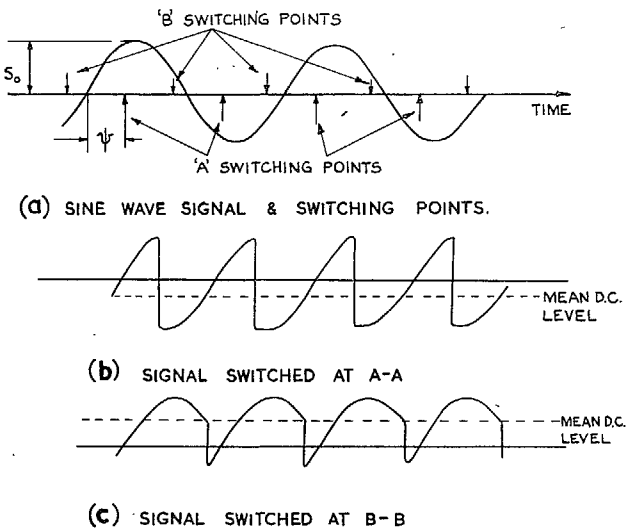

FIGS. 6a to 6c. Gauge output signal and switching.

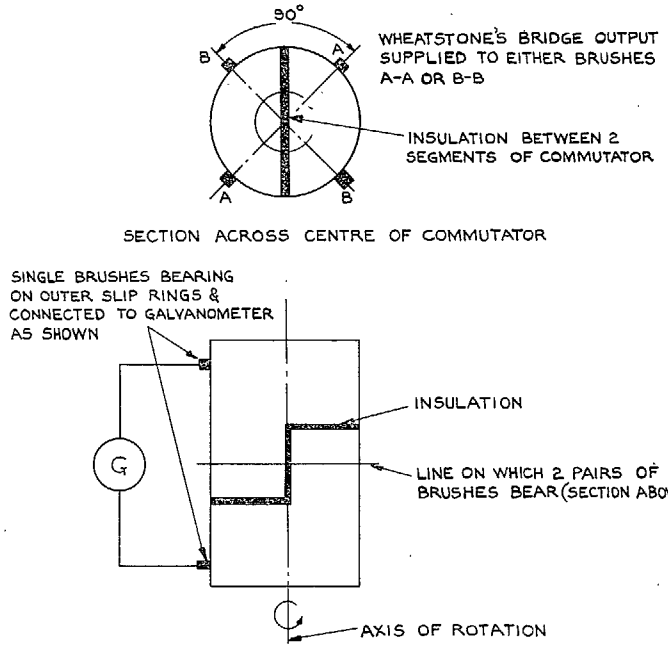

FIG. 5. Commutator and brush arrangement.

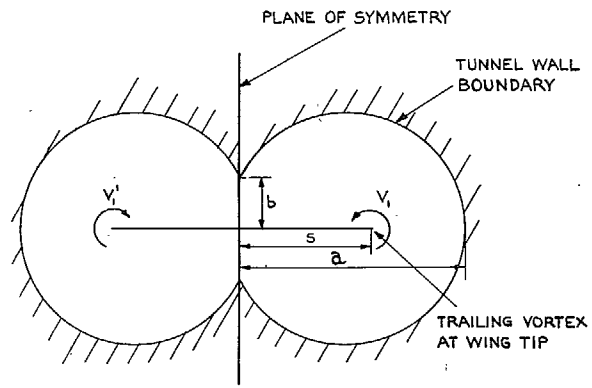

FIG. 7. Representation of wind-tunnel cross-section.

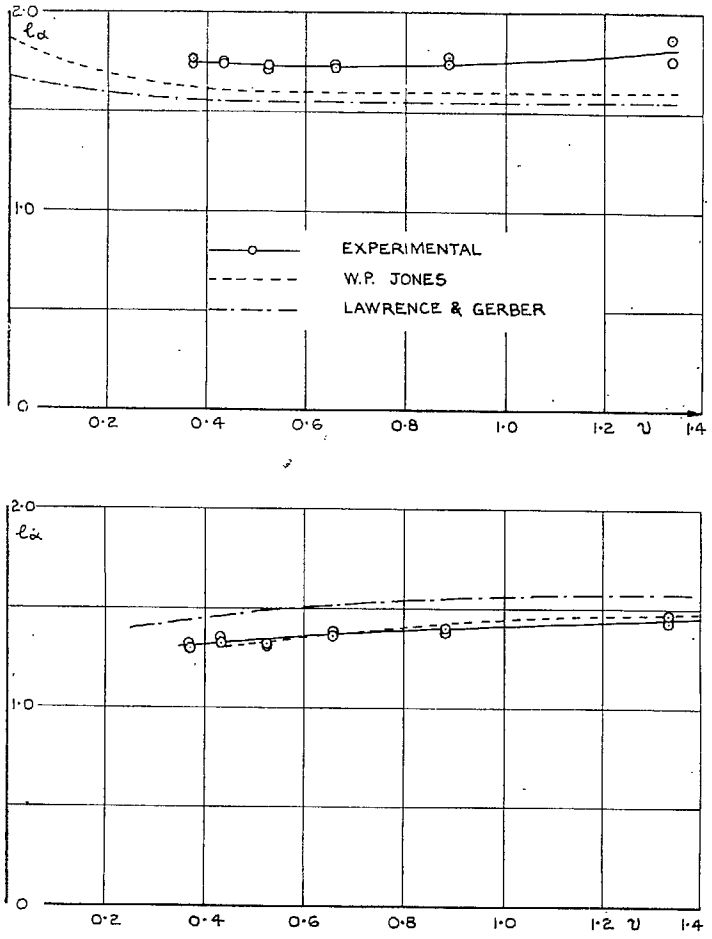

FIG. 8. Variation of l_α and $l_{\dot{\alpha}}$ with frequency parameter.

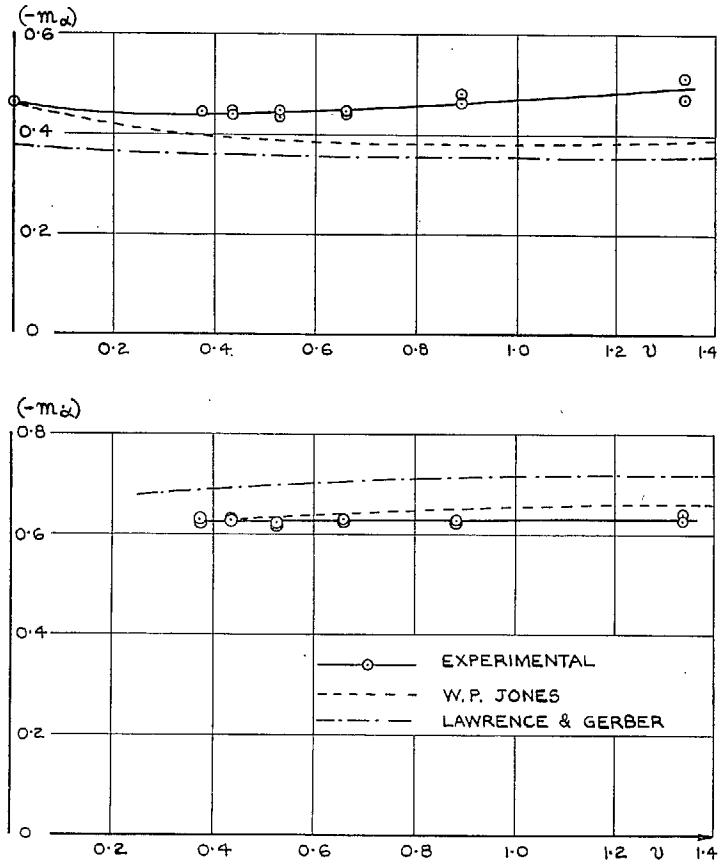

FIG. 9. Variation of $(-m_\alpha)$ and $(-m_{\dot{\alpha}})$ with frequency parameter.

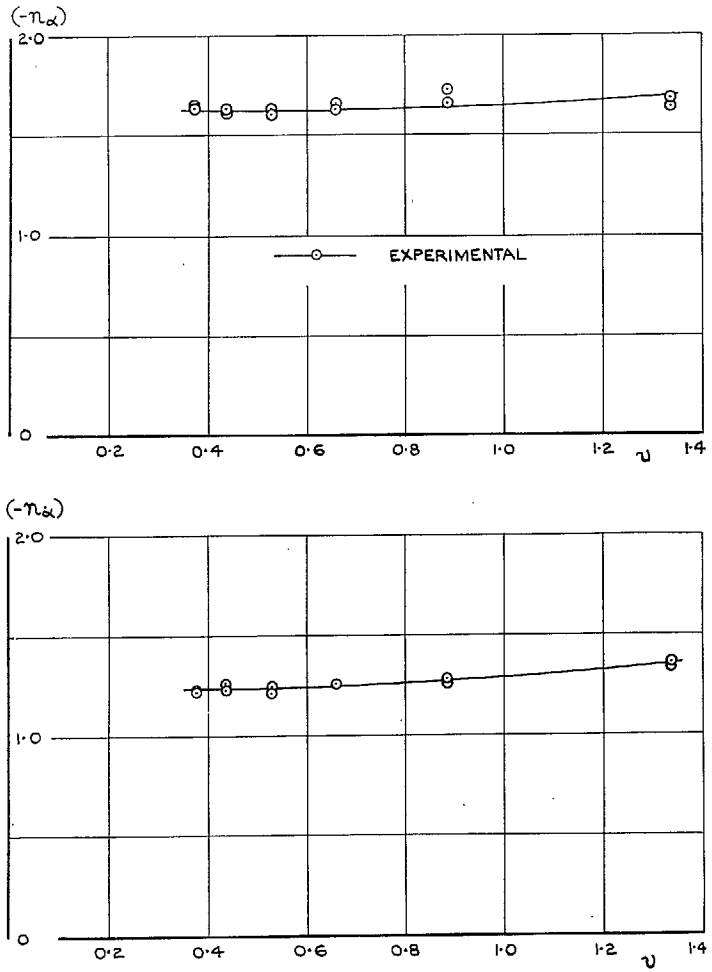

FIG. 10. Variation of $(-n_\alpha)$ and $(-n_{\dot\alpha})$ with frequency parameter.

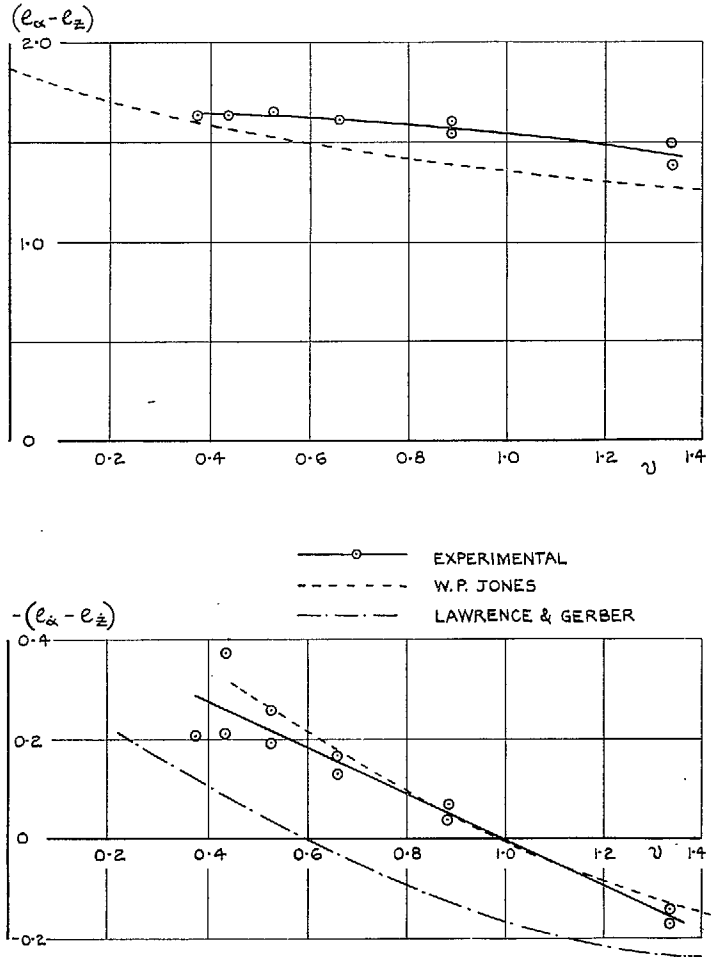

FIG. 11. Variation of $(l_\alpha - l_z)$ and $-(l_{\dot\alpha} - l_{\dot z})$ with frequency parameter.

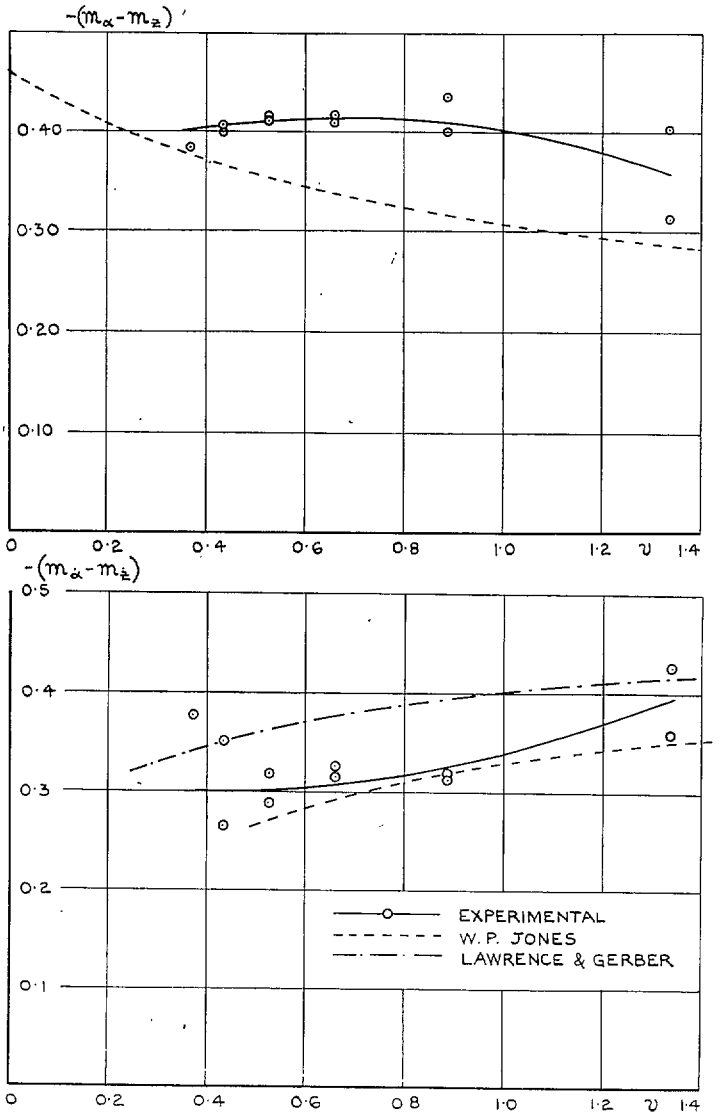

FIG. 12. Variation of $-(m_\alpha - m_z)$ and $-(m_{\dot{\alpha}} - m_{\dot{z}})$ with frequency parameter.

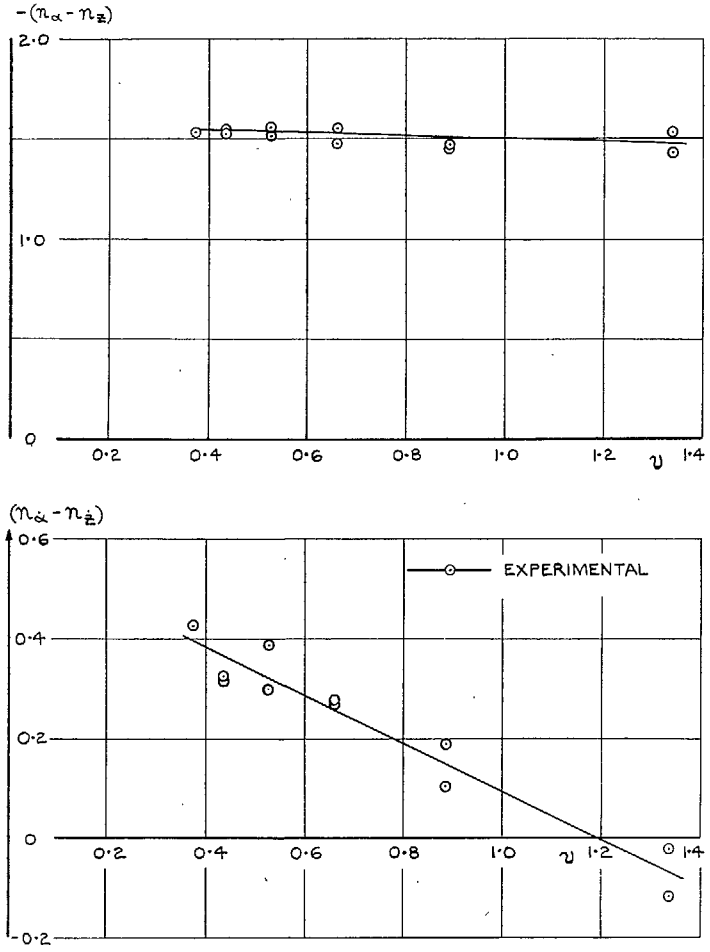

FIG. 13. Variation of $-(n_\alpha - n_z)$ and $(n_{\dot\alpha} - n_{\dot z})$ with frequency parameter.

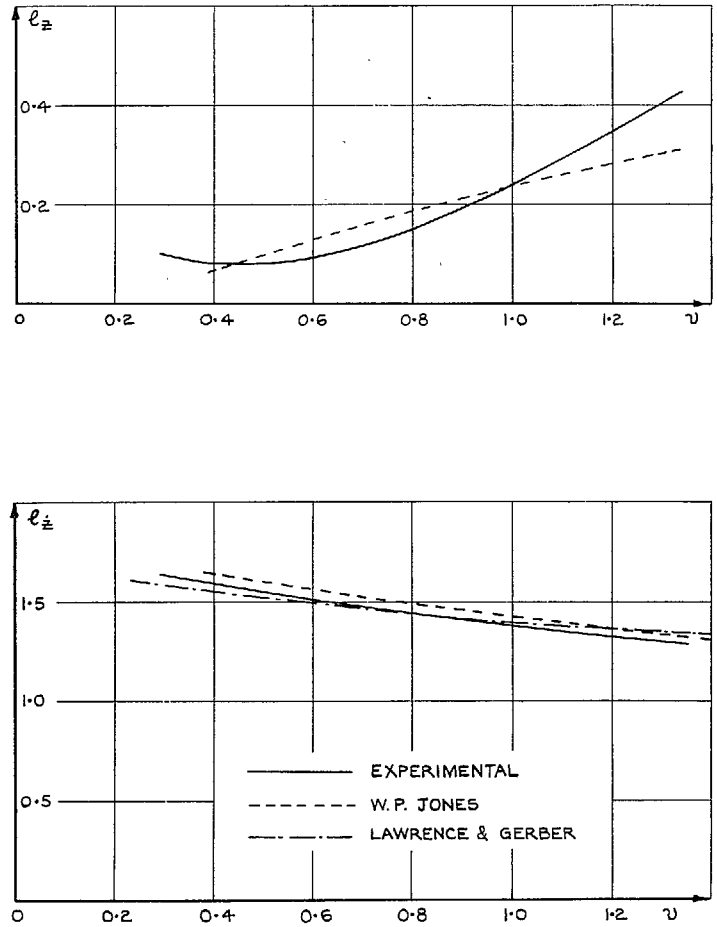

FIG. 14. Variation of l_z and $l_{\dot z}$ with frequency parameter.

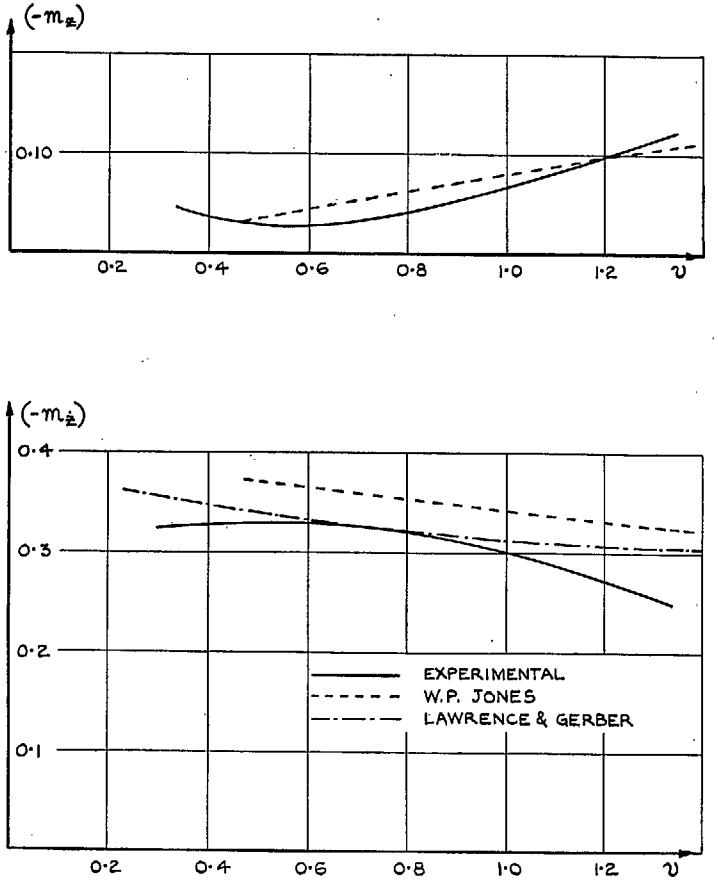

FIG. 15. Variation of $(-m_z)$ and $(-m_{\dot{z}})$ with frequency parameter.

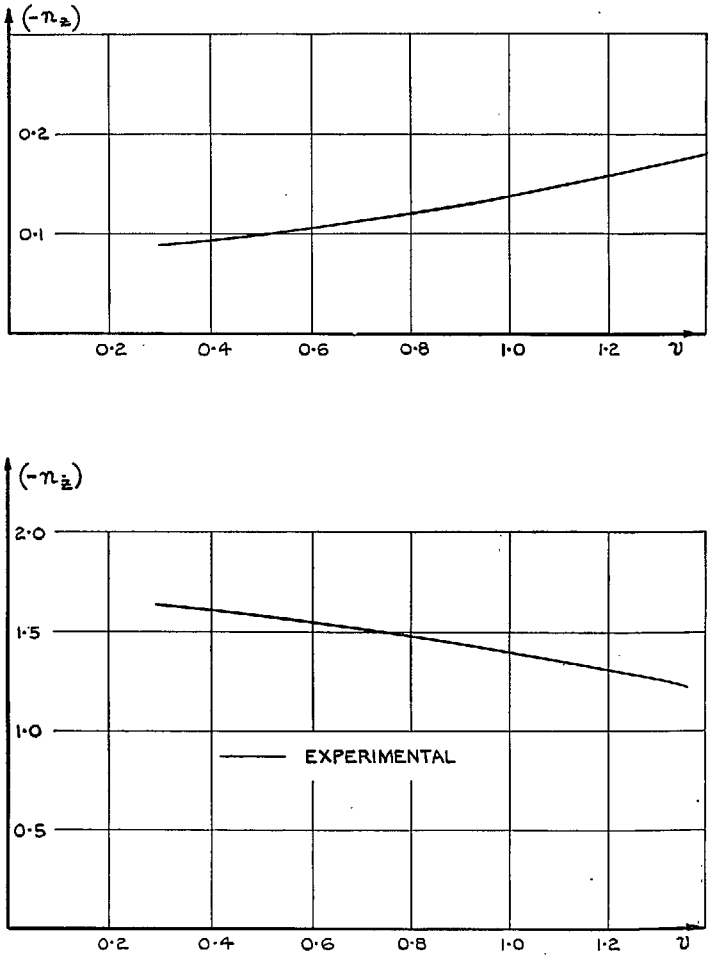

FIG. 16. Variation of $(-n_z)$ and $(-n_{\dot{z}})$ with frequency parameter.

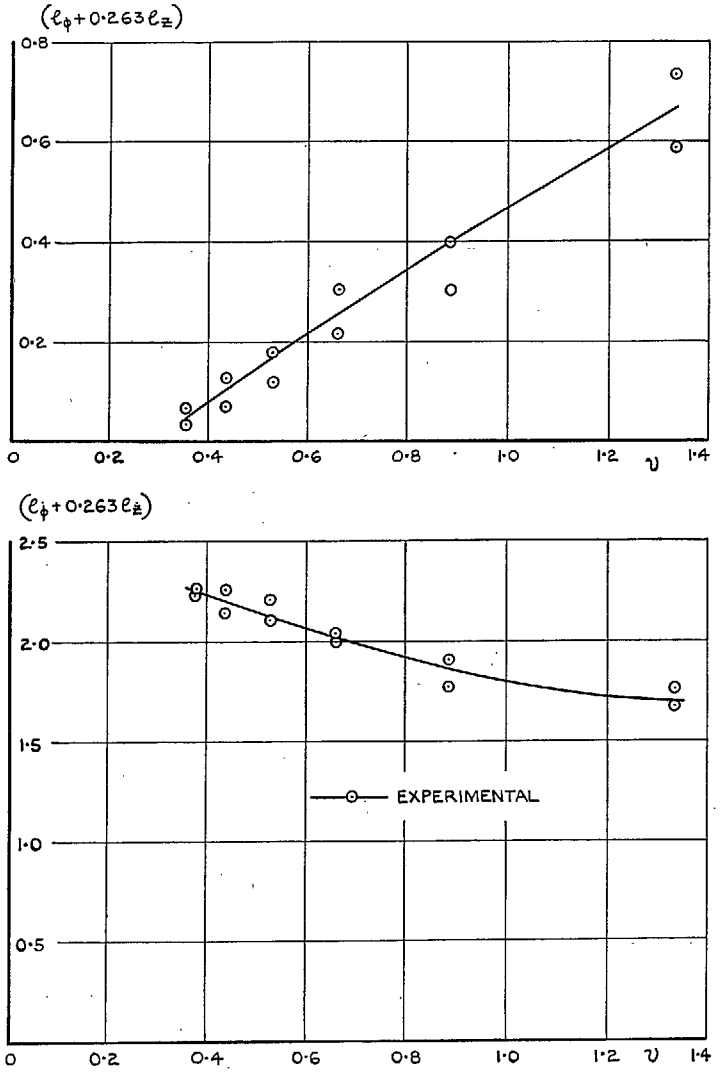

FIG. 17. Variation of $(l_\phi + 0{\cdot}263 l_z)$ and $(l_{\dot\phi} + 0{\cdot}263 l_{\dot z})$ with frequency parameter.

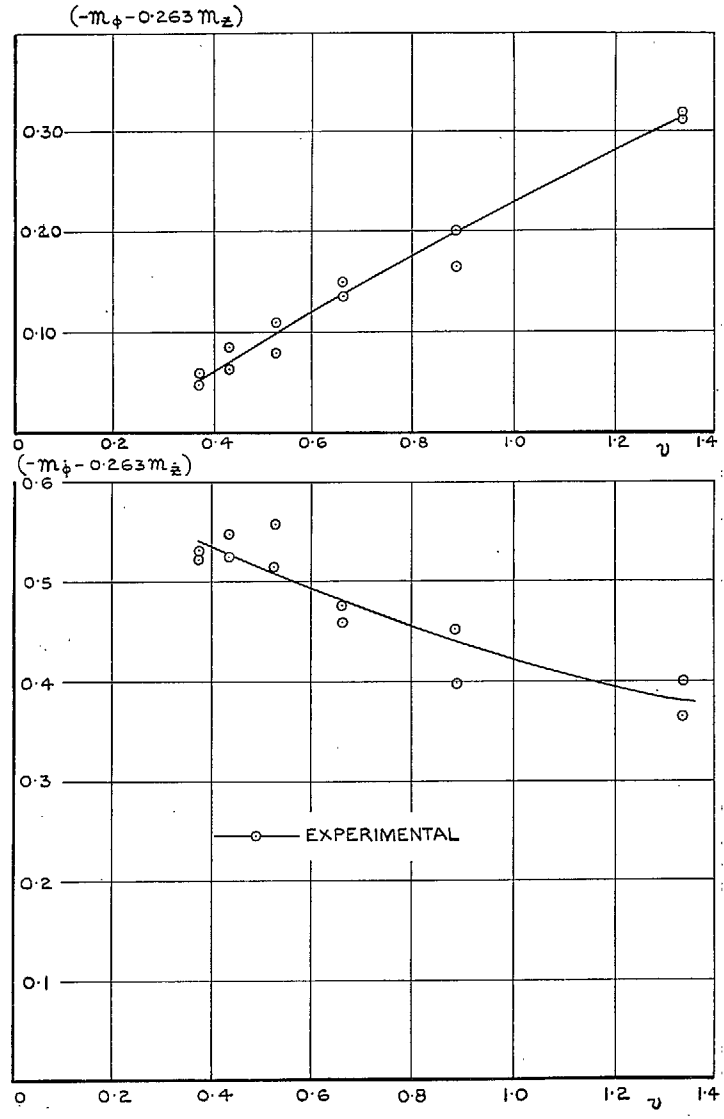

FIG. 18. Variation of $(-m_\phi - 0{\cdot}263 m_z)$ and $(-m_{\dot\phi} - 0{\cdot}263 m_{\dot z})$ with frequency parameter.

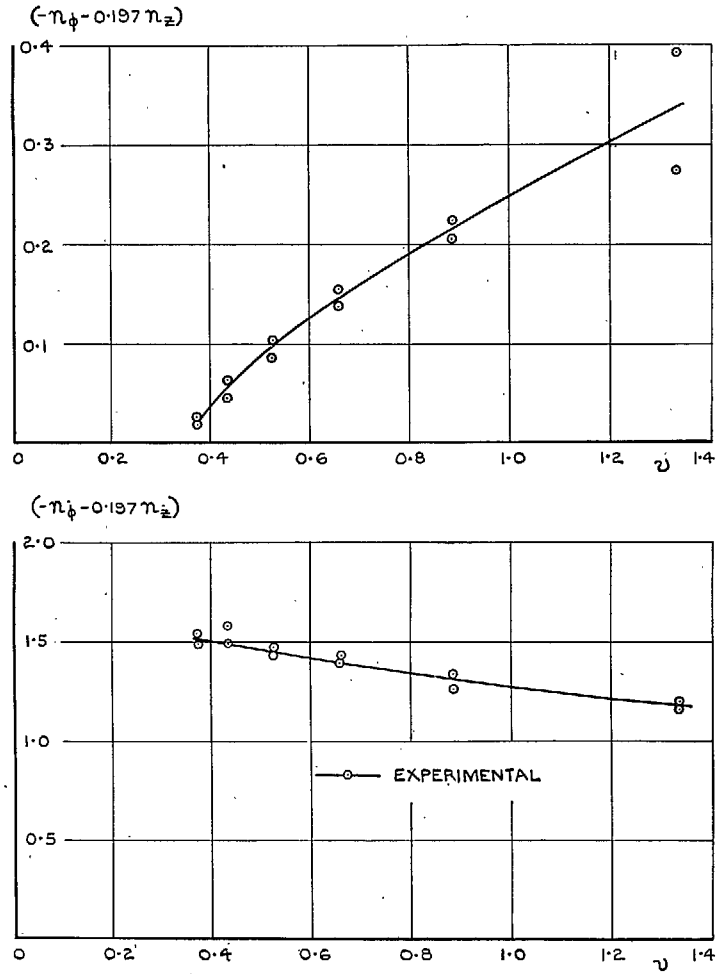

FIG. 19. Variation of $(-\, n_\phi - 0{\cdot}197 n_z)$ and $(-\, n_{\dot\phi} - 0{\cdot}197 n_{\dot z})$ with frequency parameter.

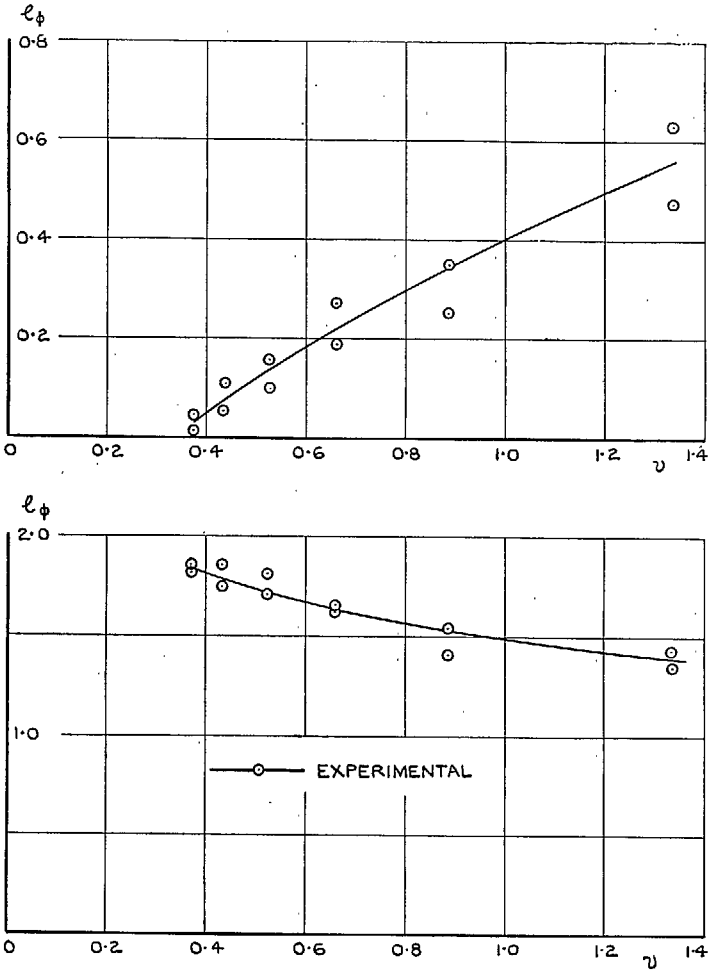

FIG. 20. Variation of l_ϕ and $l_{\dot\phi}$ with frequency parameter.

(78684) Wt. 54/8210 K.5 2/61 Hw.

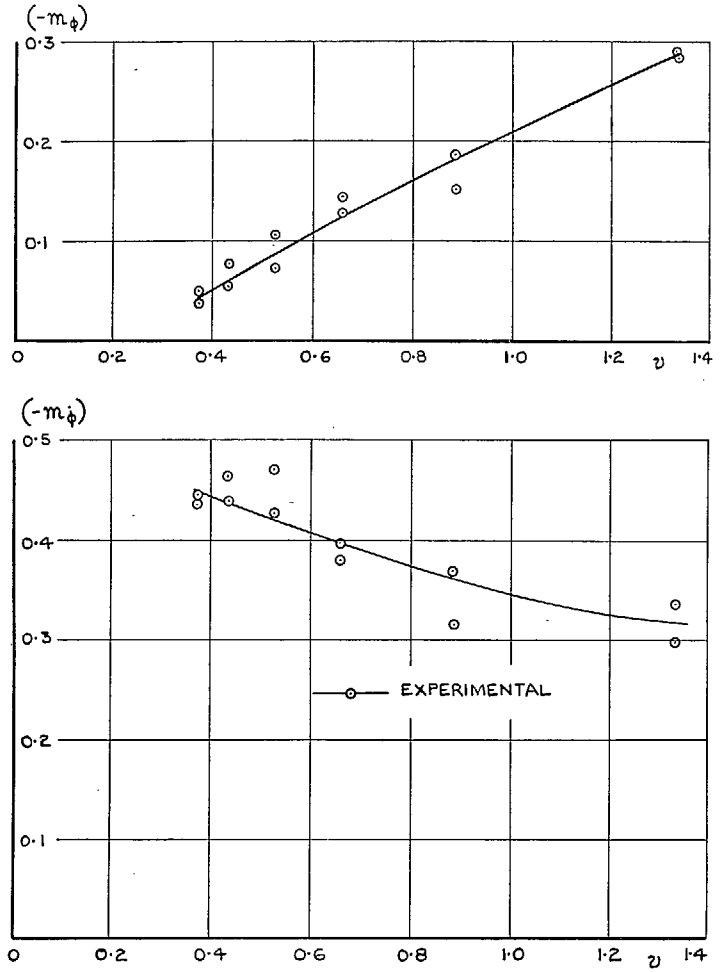

FIG. 21. Variation of $(-m_\phi)$ and $(-m_{\dot\phi})$ with frequency parameter.

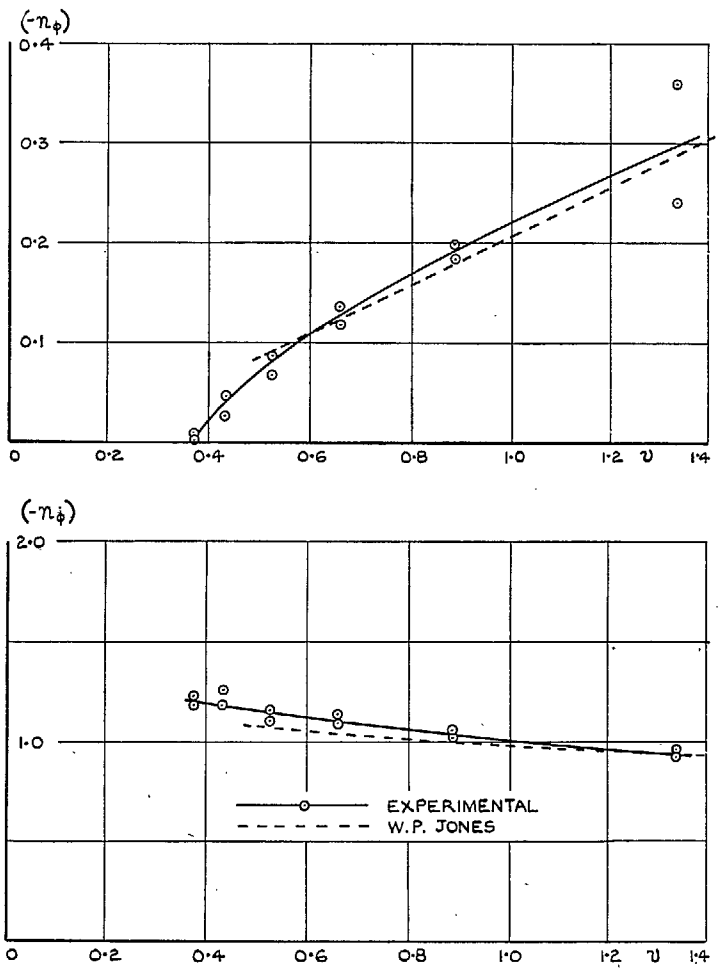

FIG. 22. Variation of $(-n_\phi)$ and $(-n_{\dot\phi})$ with frequency parameter.

Publications of the Aeronautical Research Council

ANNUAL TECHNICAL REPORTS OF THE AERONAUTICAL RESEARCH COUNCIL (BOUND VOLUMES)

1941 Aero and Hydrodynamics, Aerofoils, Airscrews, Engines, Flutter, Stability and Control, Structures. 63*s.* (post 2*s.* 3*d.*)

1942 Vol. I. Aero and Hydrodynamics, Aerofoils, Airscrews, Engines. 75*s.* (post 2*s.* 3*d.*)
Vol. II. Noise, Parachutes, Stability and Control, Structures, Vibration, Wind Tunnels. 47*s.* 6*d.* (post 1*s.* 9*d.*)

1943 Vol. I. Aerodynamics, Aerofoils, Airscrews. 80*s.* (post 2*s.*)
Vol. II. Engines, Flutter, Materials, Parachutes, Performance, Stability and Control, Structures. 90*s.* (post 2*s.* 3*d.*)

1944 Vol. I. Aero and Hydrodynamics, Aerofoils, Aircraft, Airscrews, Controls. 84*s.* (post 2*s.* 6*d.*)
Vol. II. Flutter and Vibration, Materials, Miscellaneous, Navigation, Parachutes, Performance, Plates and Panels, Stability, Structures, Test Equipment, Wind Tunnels. 84*s.* (post 2*s.* 6*d.*)

1945 Vol. I. Aero and Hydrodynamics, Aerofoils. 130*s.* (post 3*s.*)
Vol. II. Aircraft, Airscrews, Controls. 130*s.* (post 3*s.*)
Vol. III. Flutter and Vibration, Instruments, Miscellaneous, Parachutes, Plates and Panels, Propulsion. 130*s.* (post 2*s.* 9*d.*)
Vol. IV. Stability, Structures, Wind Tunnels, Wind Tunnel Technique. 130*s.* (post 2*s.* 9*d.*)

1946 Vol. I. Accidents, Aerodynamics, Aerofoils and Hydrofoils. 168*s.* (post 3*s.* 3*d.*)
Vol. II. Airscrews, Cabin Cooling, Chemical Hazards, Controls, Flames, Flutter, Helicopters, Instruments and Instrumentation, Interference, Jets, Miscellaneous, Parachutes. 168s. (post 2*s.* 9*d.*)

1947 Vol. I. Aerodynamics, Aerofoils, Aircraft. 168*s.* (post 3*s.* 3*d.*)
Vol. II. Airscrews and Rotors, Controls, Flutter, Materials, Miscellaneous, Parachutes, Propulsion, Seaplanes, Stability, Structures, Take-off and Landing. 168*s.* (post 3*s.* 3*d.*)

Special Volumes

Vol. I. Aero and Hydrodynamics, Aerofoils, Controls, Flutter, Kites, Parachutes, Performance, Propulsion, Stability. 126*s.* (post 2*s.* 6*d.*)

Vol. II. Aero and Hydrodynamics, Aerofoils, Airscrews, Controls, Flutter, Materials, Miscellaneous, Parachutes, Propulsion, Stability, Structures. 147*s.* (post 2*s.* 6*d.*)

Vol. III. Aero and Hydrodynamics, Aerofoils, Airscrews, Controls, Flutter, Kites, Miscellaneous, Parachutes, Propulsion, Seaplanes, Stability, Structures, Test Equipment. 189*s.* (post 3*s.* 3*d.*)

Reviews of the Aeronautical Research Council

1939–48 3*s.* (post 5*d.*) 1949–54 5*s.* (post 5*d.*)

Index to all Reports and Memoranda published in the Annual Technical Reports

1909–1947 R. & M. 2600 6*s.* (post 2*d.*)

Indexes to the Reports and Memoranda of the Aeronautical Research Council

Between Nos. 2351–2449	R. & M. No. 2450 2*s.* (post 2*d.*)
Between Nos. 2451–2549	R. & M. No. 2550 2*s.* 6*d.* (post 2*d.*)
Between Nos. 2551–2649	R. & M. No. 2650 2*s.* 6*d.* (post 2*d.*)
Between Nos. 2651–2749	R. & M. No. 2750 2*s.* 6*d.* (post 2*d.*)
Between Nos. 2751–2849	R. & M. No. 2850 2*s.* 6*d.* (post 2*d.*)
Between Nos. 2851–2949	R. & M. No. 2950 3*s.* (post 2*d.*)

HER MAJESTY'S STATIONERY OFFICE

from the addresses overleaf

Printed and published by
HER MAJESTY'S STATIONERY OFFICE

To be purchased from
York House, Kingsway, London W.C.2
423 Oxford Street, London W.1
13A Castle Street, Edinburgh 2
109 St. Mary Street, Cardiff
39 King Street, Manchester 2
50 Fairfax Street, Bristol 1
2 Edmund Street, Birmingham 3
80 Chichester Street, Belfast 1
or through any bookseller

Printed in England

S.O. Code No. 23-3171